INL/EXT-13-30611

Implementation of Stochastic Polynomials Approach in the RAVEN Code

Cristian Rabiti
Paul Talbot
Andrea Alfonsi
Diego Mandelli
Joshua Cogliati

October 2013

The INL is a U.S. Department of Energy National Laboratory
operated by Battelle Energy Alliance

INL/EXT-13-30611

Implementation of Stochastic Polynomials Approach in the RAVEN Code

Cristian Rabiti
Paul Talbot[1]
Andrea Alfonsi
Diego Mandelli
Joshua Cogliati

[1]Oregon State University

October 2013

Idaho National Laboratory
Idaho Falls, Idaho 83415

http://www.inl.gov

Prepared for the
U.S. Department of Energy
Office of Nuclear Energy
Under DOE Idaho Operations Office
Contract DE-AC07-05ID14517

CONTENTS

1. INTRODUCTION 3
1.1 RAVEN for Uncertainty Quantification 3

2. Generalized Polynomial Chaos 4
2.1 Generalized Polynomial Chaos by Orthonormal Expansion 4
2.1.1 Mono-Dimensional Case 4
2.1.2 Multi-Dimensional Case 6
2.2 Numerical approximation of Generalized Polynomial Chaos by Orthonormal Expansion 7
2.3 2D Application Example 9
2.3.1 From the standard to the actual reference system 9
2.3.2 Numerical evaluation of the moment integrals 12
2.3.3 Final numerical form 14
2.3.4 Mean Values 15

3. Appendixes 26
3.1 Appendix 1: Orthonormal test of the Hermite Polynomial in the actual system 26
3.2 Appendix 2: Test of the translation rule for the Gauss Hermite quadrature 27

FIGURES

Figure 1: PWR model scheme 17
Figure 2: Scheme of the electrical system of the PWR model 18
Figure 3: Max clad temperature as a function of tmin obtained sampling the system polynomial representation 21
Figure 4: Max clad temperature as a function of tmin for the original system 22
Figure 5: Stochastic Polynomials max clad temperature (2 uncertain parameters) 23
Figure 6: Limit surface from the Monte Carlo sampling of the original system 23

TABLES

Table 1: Correspondence between density function and orthogonal polynomials 6
Table 2: Legendre and Hermite first term of the series 10
Table 3: Expression for the first 3 orders of Hermite polynomials 12
Table 4: Maximum Clad Temperature Mean value 22
Table 5: Points and Weights for the Gauss-Hermite quadrature formula 27

1. INTRODUCTION

1.1 RAVEN for Uncertainty Quantification

RAVEN, under the support of the Nuclear Energy Advanced Modeling and Simulation program, has been tasked to provide the necessary software and algorithms to enable the application of the conceptual framework developed by the Risk Informed Safety Margin Characterization (RISMC) [1] path. RISMC is one of the paths defined under the Light Water Reactor Sustainability Department of Energy program [2].

One of the most challenging requests of the RISMC framework is a holistic estimation of margins, and therefore uncertainties, in nuclear power plant system analysis. Those estimations, in conjunction with more accurate simulation tools, should enable an optimization process leading to safer and more economical competitive nuclear power plants.

The improvement of the accuracy of the simulations is tasked to other Department of Energy projects like RELAP-7 [3], while margin quantification and the generation of information suitable to perform safety margin managements is assigned to RAVEN.

How the uncertainty of the input parameters impacts the simulation results (uncertainty propagation) is clearly a fundamental step of the process. The uncertainty propagation analysis is a complex process and several methodologies are currently used. Before deploying innovative algorithms, base capabilities need to be implemented and tested. This is the current stage of the RAVEN development project.

Earlier reports [4] show the implementation of Monte Carlo sampling methodologies in RAVEN and dynamic event trees [5]. The next step of this strategy is described here and involves the implementation of the infrastructure to support the generalized Polynomial Chaos [6] methodology for uncertainty propagation.

In this report, we will cover the following subjects: introduction of the generalized Stochastic Polynomial approach, exemplification of the approach in a bi-dimensional case, results of the implementation tests, and a direct comparison toward a Monte Carlo approach for the estimation of the maximum fuel temperature in a simplified Station Blackout (SBO) pressurized water reactor (PWR) accident scenario.

2. Generalized Polynomial Chaos

2.1 Generalized Polynomial Chaos by Orthonormal Expansion

2.1.1 Mono-Dimensional Case

Of the large amount of literature on stochastic polynomials, a good starting point is provided by Xiu and Karniadakis [6]. We present a brief introduction focused on the implementation strategy.

In general, any response (**U**) monitored at the plant (clad temperature, max pressure etc.) at a given point in time may be represented as a function of the initial condition of the plant and of the values of the parameters used to construct the mathematical models. For our purpose, we consider a split of the input and parameter space, such that $\bar{p}$ are the initial conditions and parameters not subjected to a probabilistic distribution, while $\bar{\xi}$ are the ones showing such stochastic behavior. The dependence of U from $\bar{p}$ could be therefore neglected since the dependence is not relevant to the discussion:

$$U = U(\bar{\xi})$$

Eq. 2-1

Next, we introduce the Lebesgue space equipped with measure μ (for simplicity, we assume a one-dimensional problem $\bar{x} = x$):

$$L^2(S,\mu) = \left\{ f(\xi) | \int_S f(\xi)^2 d\mu < \infty \right\},$$

Eq. 2-2

with S being the support of the measure. The scalar product in such space is therefore:

$$\big(f(\xi), g(\xi)\big)_\mu = \int_S f(\xi) g(\xi) d\mu(\xi),$$

Eq. 2-3

or, under the assumption that the measure admits a density function $\rho(\xi)\mathrm{d}\xi = \mathrm{d}\mu(\xi)$:

$$\big(f(\xi), g(\xi)\big)_\mu = \big(f(\xi), g(\xi)\big)_{\rho(\xi)} = \int_S f(\xi) g(\xi) \rho(\xi) d\xi.$$

Eq. 2-4

Now, if $\{B_i(\xi)\}$ is a complete function based on $\mathrm{L}^2(S,\mu)$, the Fourier theorem ensures that the equality

$$U(\xi) = \sum_{n=0}^{\infty} c_n B_n(\xi)$$

Eq. 2-5

is respected in the μ norm if the moment c_n of the series is defined as follows:

$$c_n = \frac{\big(U(\xi), B_n(\xi)\big)_{\rho(\xi)}}{\big(B_n(\xi), B_n(\xi)\big)_{\rho(\xi)}} = \frac{\int_S U(\xi) B_n(\xi) \rho(\xi) d\xi}{\int_S B_n(\xi) B_n(\xi) \rho(\xi) d\xi}.$$

Eq. 2-6

If $B_n(\xi)$ is an orthonormal base in $\mathrm{L}^2(S,\mu)$, we have:

$$\int_S B_m(\xi)B_n(\xi)\rho(\xi)d\xi = \delta_{m,n}, c_n = \int_S U(\xi)B_n(\xi)\rho(\xi)d\xi,$$

Eq. 2-7

and in fact:

$$c_n = \int_S U(\xi)B_n(\xi)\rho(\xi)d\xi = \int_S \sum_{n'=0}^{\infty} c_{n'}B_{n'}(\xi)\, B_n(\xi)\rho(\xi)d\xi =$$
$$= \sum_{n'=0}^{\infty} c_{n'} \int_S B_{n'}(\xi)B_n(\xi)\rho(\xi)d\xi = \delta_{n',n}c_{n'} = c_n.$$

To reformulate the problem in L^2 space with a standard measure, it is sufficient to replace $B_n(\xi)$ with $\tilde{B}_n(\xi)$, where:

$$\tilde{B}_n(\xi) = B_n(\xi)\sqrt{\rho(\xi)}$$

Eq. 2-8

$$\tilde{c}_n = \int_S U(\xi)\tilde{B}_n(\xi)d\xi \int_S U(\xi)B_n(\xi)\sqrt{\rho(\xi)}d\xi$$

Eq. 2-9

Clearly, the orthonormal property of $B_n(\xi)$ over $L^2(S, \mu)$ translates in the orthonormal property for $\tilde{B}_n(\xi)$ over $L^2(S, \xi)$. The introduction of the $L^2(S, \mu)$ space finds its utility when the measure is defined as:

$$pdf(\xi) = \sqrt{\rho(\xi)}.$$

In this case, the expected value of $U(\xi)$ $(E[U(\xi)])$ has an immediate formulation with respect to the term of the Fourier series:

$$E[U(\xi)] = \int_S U(\xi)pdf(\xi)d\xi = \int_S \sum_{n=0}^{\infty} c_n\tilde{B}_n(\xi)\sqrt{\rho(\xi)}d\xi$$
$$= \int_S \sum_{n=0}^{\infty} c_nB_n(\xi)\,\rho(\xi)d\xi = \int_S \sum_{n=0}^{\infty} c_nB_n(\xi)\, B_0(\xi)\sqrt{S}\rho(\xi)d\xi = B_0\sqrt{S};$$

Eq. 2-10

where these properties are used:

$$\tilde{B}_n(\xi) = B_n(\xi)\sqrt{\rho(\xi)},$$
$$B_0(\xi) = \frac{1}{\sqrt{S}}$$

Eq. 2-11

with $\frac{1}{\sqrt{S}}$ as the normalization constant for the polynomial of order 0 where S=$\int_S \rho(\xi)d\xi$.

In

Table 1, the most common distribution functions are paired with their respective orthonormal polynomials.

Table 1: Correspondence between density function and orthogonal polynomials.

Distribution	*Probability Distribution Function*	*Polynomials*	*Support*
Uniform	$1/2$	Legendre	$[-1:1]$
Normal	$\frac{1}{\sigma\sqrt{2\pi}} e^{-\frac{(x-m)^2}{2\sigma^2}}$	Hermite	$[-\infty:\infty]$
Exponential	e^{-x}	Laguerre	$[0:\infty]$
Beta	$x^{\alpha-1}(1-x)^{\beta-1}$	Jacobi	$[-1:1]$

2.1.2 Multi-Dimensional Case

The extension to the multi-dimensional case has no special complication if care is used in merging the different density functions. As in the mono-dimensional case, we can introduce the following Lebesgue space:

$$\mathrm{L}^2(S,\mu) = \left\{ f(\bar{\xi}) | \int_S f(\bar{\xi})^2 \mathrm{d}\mu(\bar{\xi}) \right\}$$

Eq. 2-12

If $dim[\{\bar{\xi}\}] = L$, we define first the multi-dimensional polynomial base using vector indexing: $\bar{n} \in \{(n_1,..,n_L)\} = N^L$ to obtain the expansion of $U(\bar{\xi})$ so that:

$$B_{\bar{n}} = \prod_{l=1}^{L} B_{n_l}(\xi_l),$$

Eq. 2-13

$$c_{\bar{n}} = \int_S U(\bar{\xi}) \left(\prod_{l=1}^{L} B_{n_l}(\xi_l) \right) \rho(\bar{\xi}) d\bar{\xi} = \int_S U(\bar{\xi}) B_{\bar{n}} \rho(\bar{\xi}) d\bar{\xi},$$

Eq. 2-14

$$\tilde{B}_{\bar{n}}(\bar{\xi}) = \sqrt{\rho(\bar{\xi})} \prod_{l=1}^{L} B_{n_l}(\xi_l),$$

Eq. 2-15

$$\tilde{c}_{\bar{n}} = \int_S U(\bar{\xi}) \left(\prod_{l=1}^{L} B_{n_l}(\xi_l) \right) \sqrt{\rho(\bar{\xi})} d\bar{\xi};$$

Eq. 2-16

where the polynomial has already been assumed to be orthonormal. Then the expansion series is similar to what we found in the one-dimensional case:

$U(\bar{\xi}) = \sum_{\bar{n}=\emptyset}^{\infty} c_{\bar{n}} B_{\bar{n}}(\bar{\xi})$ in the μ norm,
and $U(\bar{\xi}) = \sum_{\bar{n}=\emptyset}^{\infty} \tilde{c}_{\bar{n}} \tilde{B}_{\bar{n}}(\bar{\xi})$ in the standard norm.

Many times, the probability distributions of the input parameters $(\bar{\xi})$ are uncorrelated, and therefore, if we impose that the density function of the measure is the Cumulative Distribution Function of those random variates, it follows that the density function is (completely) multiplicatively separable (completeness is true, of course, if all the input variables are uncorrelated).

For completely multiplicatively separable density functions, the construction of the orthonormal base in the multi-dimensional space, with respect the standard measure $d\bar{\xi}$, is straightforward:

$$\rho(\bar{\xi}) = \prod_{l=1}^{L} \sqrt{\rho(\xi_l)}$$

$$\tilde{B}_{\bar{n}} = \prod_{l=1}^{L} B_{n_l}(\xi_l)\sqrt{\rho(\xi_l)}$$

$$\tilde{c}_{\bar{n}} = \int_S U(\bar{\xi}) \left(\prod_{l=1}^{L} B_{n_l}(\xi_l) \sqrt{\rho_l((\xi_l))} d\xi_l \right)$$

Eq. 2-17

Another interesting discriminant for approaching the construction of the orthonormal polynomial base is provided by the existence of a vector sub space ($\Theta \in \{\bar{\xi}\}$), such as the directional derivative of the density function equaling zero whenever $\bar{\omega} \in \Theta$. If such a linear space exists, then the effective dimensionality of the input space could be reduced and the study of the function $U(\bar{\xi})$ could be correspondingly simplified. For this report, this condition will not be investigated further, but it could be very useful when the input space is representative of a physical field. For cases when the dimension of Θ is rather large but strongly correlated, reducing the effort required to represent the original $U(\bar{\xi})$ function is possible and highly advantageous.

2.2 Numerical Approximation of Generalized Polynomial Chaos by Orthonormal Expansion

The first step toward achieving a numerical approximation of the stochastic expansion of the $U(\bar{\xi})$ is introducing a finite expansion approximation over the orthonormal polynomial base. If N_l is the maximum polynomial order over the variable ξ_l, than the cardinality of $\bar{n}$ is $[\bar{n}] = \prod_{l=1}^{L} N_l$, and the function $U(\bar{\xi})$ could be approximated by:

$$U(\bar{\xi}) = \sum_{\bar{n}=0}^{(N_1, \ \ldots, \ N_L)} c_{\bar{n}} B_{\bar{n}} \left(\mu(\bar{\xi})\right) \text{ in the } \mu \text{ norm},$$

$$U(\bar{\xi}) = \sum_{\bar{n}=0}^{[N_1, \ \ldots, \ N_L]} \tilde{c}_{\bar{n}} \tilde{B}_{\bar{n}}(\bar{\xi}) \text{ in the standard norm.}$$

Eq. 2-18

For simplicity, we can assume that the density function is completely multiplicatively separable. This simplification does not affect the substance of the following derivation since this condition is always achievable by a truncated development over a proper base on $L^2(S, \bar{\xi})$ or a suitable variable change. The definition of the moment rests unaltered from Eq. 2-17.

Moreover, we can rewrite $U(\bar{\xi})$ as follows:

$$U(\bar{\xi}) \approx \sum_{\bar{n}=0}^{[N_1,\ \ldots,\ N_L]} \tilde{c}_{\bar{n}} \tilde{B}_{\bar{n}}(\bar{\xi}) = \sum_{\bar{n}=0}^{[N_1,\ \ldots,\ N_L]} \tilde{c}_{\bar{n}} \prod_{l=1}^{L} B_{n_l}(\xi_l)\sqrt{\rho(\xi_l)} = \prod_{l=1}^{L}\left(\sum_{n=0}^{N_l} \tilde{c}_{n_l} B_{n_l}(\xi_l)\sqrt{\rho(\xi_l)}\right)$$
$$= \prod_{l=1}^{L} U_l(\xi_l).$$

Eq. 2-19

Where:

$$U_l(\xi_l) = \sum_{n=0}^{N_l} \tilde{c}_{n_l} B_{n_l}(\xi_l)\sqrt{\rho(\xi_l)}\,\tilde{c}_{n_l} = \int_{S_l} U_l(\xi_l) B_{n_l}(\xi_l)\sqrt{\rho(\xi_l)}\,d\xi_l$$

Eq. 2-20

Once a proper finite polynomial representation $\left\{B_{n_l}(\xi_l)\sqrt{\rho(\xi_l)}\right\}$ has been chosen to represent $U(\bar{\xi})$, the main task is the calculation of $\tilde{c}_{n_l}$. Two approaches could be followed; one relies on a projection of the equation set representing the system of which $U(\bar{\xi})$ is solution on $B_{n_l}(\xi_l)\sqrt{\rho(\xi_l)}$. Usually this leads to a hierarchical system of equations with unknown $\tilde{c}_{n_l}$. The second approach seeks a numerical solution of the integral representing the $\tilde{c}_{n_l}$ by the knowledge of $U_l(\xi_l)B_{n_l}(\xi_l)\sqrt{\rho(\xi_l)}$ for specific point of the input domain $\xi_{l,i}$. The second methodology is the one currently implemented in RAVEN since it does not require the alteration of the software solving for $U(\bar{\xi})$, which is, in our case, RELAP-7. Given that this second methodology relies on the knowledge of the $U(\bar{\xi})$ only at selected points, it is named Collocation Generalized Polynomial Chaos [7].

Of course, the choice of the points where the function $U_l(\xi_l)B_{n_l}(\xi_l)\sqrt{\rho(\xi_l)}$ is evaluated could be optimized to minimize the number of code runs needed while maximizing the order of the polynomial representation achievable. This is obtained by the Gauss integration rule pertinent to the orthonormal polynomial set under consideration. In general, using the Gauss integration 'p' points will integrate exactly a polynomial of order n=2p-1. It is important to recognize that the integrand that appears in the definition of $\tilde{c}_{N_l}$ is of degree $2N_l$, in fact:

$$\tilde{c}_{N_l} = \int_{S_l} U_l(\xi_l) B_{N_l}(\xi_l)\sqrt{\rho(\xi_l)}\,d\xi_l = \int_{S_l}\left(\sum_{n'=0}^{N_l} \tilde{c}_{n_l} B_{n_l}(\xi_l)\sqrt{\rho(\xi_l)}\right) B_{N_l}(\xi_l)\sqrt{\rho(\xi_l)}\,d\xi_l,$$

Eq. 2-21

where the integrand of highest degree is $\left(B_{N_l}(\xi_l)\right)^2$. This implies that to achieve an overall accuracy of degree N_l, it is necessary to have a minimum number of points satisfy $p \geq N_l + 1$ (rounding ½ to 1 is the consequence of the number of point being an integer).

3. 2D Application Example

It is useful to illustrate the methodology with a two-dimensional example. Consider a system response ($\bar{\xi}$) mapped as a function of two random variates (x, y). Moreover, assume it is completely multiplicatively separable, so $\bar{\xi} = \xi_x \xi_y$. The corresponding probability density, density, and measure of the support in the corresponding metrics are provided below:

$$pdf(x) = \frac{1}{\sigma\sqrt{2\pi}} e^{-\frac{(x-m)^2}{2\sigma^2}}, \qquad pdf(y) = \frac{1}{(y_b - y_a)},$$

$$\rho_x(x) = \frac{1}{\sigma^2 2\pi} e^{-\frac{(x-m)^2}{\sigma^2}}, \qquad \rho(y) = \frac{1}{(y_b - y_a)^2},$$

$$S_x = \int_{-\infty}^{\infty} \rho(x)dx = \frac{1}{\sigma^2 2\pi} \int_{-\infty}^{\infty} e^{-\frac{(x-m)^2}{\sigma^2}} dx = \frac{1}{\sigma^2 2\pi} \sigma\sqrt{\pi} = \frac{1}{\sigma 2\sqrt{\pi}},$$

$$S_y = \int_{y_a}^{y_b} \rho(y)dy = \frac{1}{(y_b - y_a)^2} \int_{y_a}^{y_b} dy = \frac{1}{(y_b - y_a)}.$$

Eq. 3-1

3.1.1 From the Standard to the Actual Reference System

The orthonormal polynomials needed in our case are the ones that satisfy the following orthonormal conditions:

$$\frac{1}{\sigma^2 2\pi} \int_{-\infty}^{\infty} He_m(x) He_n(x) e^{-\frac{(x-m)^2}{\sigma^2}} dx = \delta_{m,n}, \qquad \frac{1}{(y_b - y_a)^2} \int_{y_a}^{y_b} L_m(x) L_n(x) dx = \delta_{m,n}.$$

Eq. 3-2

Since these are not available in the literature, generic forms are provided for standardized ρ. Using these forms, it is possible to derive ones needed in other specific cases. In this specific case, we need a set of normal polynomials with respect to the class of weighting function represented by $e^{-\alpha x^2}$ and constant values that respectively are given by the Hermite and Legendre polynomials. The expression of the first few terms of their standard series is provided in Table 2 along with the orthonormal conditions.

Table 2: Legendre and Hermite first term of the series.

Order	Hermite	Legendre
0	$\frac{1}{\sqrt[4]{2\pi}}$	$\frac{1}{\sqrt{2}}$
1	$x'\frac{1}{\sqrt[4]{2\pi}}$	$x'\frac{\sqrt{3}}{\sqrt{2}}$
2	$(x'^2-1)\frac{1}{\sqrt[4]{2\pi}\sqrt{2}}$	$(3x'^2-1)\sqrt{2}\sqrt{5}$
3	$(x'^3-3x')\frac{1}{\sqrt[4]{2\pi}\sqrt{6}}$	$(5x'^3-3x')\sqrt{2}\sqrt{7}$
Orthonormal condition	$\int_{-\infty}^{\infty} He'_n(x')He'_m(x')e^{-\frac{x'^2}{2}}dx' = \delta_{m,n}$	$\int_{-1}^{1} L'_n(x')L'_m(x')dx' = \delta_{m,n}$

The following coordinate changes are applied to obtain the needed polynomials:

Hermite

$$x' = \frac{\sqrt{2}(x-m)}{\sigma},$$
$$x = \frac{\sigma}{\sqrt{2}}x' + m,$$

Legendre

$$y' = \frac{2y - (y_b + y_a)}{(y_b - y_a)},$$
$$y = \frac{(y_b - y_a)}{2}y' + \frac{(y_b + y_a)}{2},$$

Eq. 3-3

By applying these coordinate changes in the orthonormal conditions, it is possible to derive the relationship between the polynomials in the actual (x, y) system and in the reference one (x', y').

Hermite:

First, the coordinate transformation is applied into the orthonormal condition for the standard system in Table 2:

$$\frac{\sigma^2 2\pi\sqrt{2}}{\sigma}\int_{-\infty}^{\infty} He'_n\left(\frac{\sqrt{2}(x-m)}{\sigma}\right)He'_m\left(\frac{\sqrt{2}(x-m)}{\sigma}\right)\frac{1}{\sigma^2 2\pi}e^{-\frac{(x-m)^2}{\sigma^2}}dx = \delta_{m,n}.$$

To satisfy Eq. 3-2, $He_m(x)$ has to be expressed by:

$$He_m(x) = He'_m(x'(x))\sqrt{\sigma 2\pi\sqrt{2}} = He'_m\left(\frac{\sqrt{2}(x-m)}{\sigma}\right)\sqrt{\sigma 2\pi\sqrt{2}}.$$

Eq. 3-4

$He_m(x)$ is therefore orthonormal over $[-\infty, \infty]$ with density function $\frac{1}{\sigma^2 2\pi}e^{-\frac{(x-m)^2}{\sigma^2}}$, and $\widetilde{He}_m(x)$ is orthonormal over the standard norm with support $[-\infty, \infty]$ and defined by:

$$\widetilde{He}_m(x) = He_m(x)\frac{1}{\sigma\sqrt{2\pi}}e^{-\frac{(x-m)^2}{2\sigma^2}} = He'_m\left(\frac{\sqrt{2}(x-m)}{\sigma}\right)\sqrt{\sigma 2\pi\sqrt{2}}\frac{1}{\sigma\sqrt{2\pi}}e^{-\frac{(x-m)^2}{2\sigma^2}}$$
$$= He'_m\left(\frac{\sqrt{2}(x-m)}{\sigma}\right)\frac{\sqrt[4]{2}}{\sqrt{\sigma}}e^{-\frac{(x-m)^2}{2\sigma^2}}.$$

Eq. 3-5

This derivation is checked against the orthonormal condition for a few moment integrals in appendix 1.

Legendre:

Recasting the standard Legendre polynomials from Table 2 $L_n(y')$ following the coordinate transformation in Eq. 3-3 leads to:

$$2(y_b - y_a)\int_{y_a}^{y_b} L'_m(y'(y))L'_n(y'(y))\frac{1}{(y_b - y_a)^2}dy = \delta_{m,n}.$$

Eq. 3-6

The normalization condition to satisfy Eq. 3-2 is therefore met by posing:

$$L_m(y) = L'_m(y'(y))\sqrt{2(y_b - y_a)} = L'_m\left(\frac{2y - (y_b + y_a)}{(y_b - y_a)}\right)\sqrt{2(y_b - y_a)}.$$

Eq. 3-7

$L_m(y)$ is consequently orthonormal over $[y_a, y_b]$ with density function $\frac{1}{(y_b - y_a)^2}$, and

$$\tilde{L}_m(y) = L_m(y)\frac{1}{(y_b - y_a)} = L_m\left(\frac{2y - (y_b + y_a)}{(y_b - y_a)}\right)\sqrt{\frac{2}{(y_b - y_a)}}$$

Eq. 3-8

is orthonormal over $[y_a, y_b]$ with the standard measure.

It is required in this case to verify that $\int_{y_a}^{y_b} L_0(y)L_0(y)\frac{1}{(y_b - y_a)^2}dx$=1:

$$L'_0(y') = \frac{1}{\sqrt{2}}, L_0(y) = \frac{\sqrt{2(y_b - y_a)}}{\sqrt{2}} = \sqrt{(y_b - y_a)}, \widetilde{L_0}(y) = \frac{1}{\sqrt{(y_b - y_a)}},$$

$$\int_{y_a}^{y_b} L_0(y)L_0(y)\frac{1}{(y_b - y_a)^2}dx = \int_{y_a}^{y_b}\sqrt{(y_b - y_a)}\sqrt{(y_b - y_a)}\frac{1}{(y_b - y_a)^2}dx = \frac{1}{(y_b - y_a)}\int_{y_a}^{y_b} dx.$$

Now that the new orthonormal polynomials have been defined using the polynomials in the reference system and the change of coordinates described by Eq. 3-3, the expansion series becomes:

$$\bar{\xi} = \xi_x\xi_y = \left[\sum_{n_x=0}^{N_x}\xi_{n_x}\left(He_{n_x}(x)\frac{1}{\sigma\sqrt{2\pi}}e^{-\frac{(x-m)^2}{2\sigma^2}}\right)\right]\left[\sum_{n_y=0}^{N_y}\xi_{n_y}\left(L_{n_y}(y)\frac{1}{(y_b - y_a)}\right)\right]$$
$$= \left[\sum_{n_x=0}^{N_x}\xi_{n_x}\left(He'_m\left(\frac{\sqrt{2}(x-m)}{\sigma}\right)\frac{\sqrt[4]{2}}{\sqrt{\sigma}}e^{-\frac{(x-m)^2}{2\sigma^2}}\right)\right]\left[\sum_{n_y=0}^{N_y}\xi_{n_y}\left(L'_m\left(\frac{2y - (y_b + y_a)}{(y_b - y_a)}\right)\sqrt{\frac{2}{(y_b - y_a)}}\right)\right].$$

Eq. 3-9

Where the moments are expressed by:

$$\xi_{n_x} = \int_{-\infty}^{\infty} \xi_x(x)\tilde{He}_{n_x}(x)dx = \int_{-\infty}^{\infty} \xi_x(x)He_{n_x}(x)\frac{1}{\sigma\sqrt{2\pi}}e^{-\frac{(x-m)^2}{2\sigma^2}}dx$$
$$= \int_{-\infty}^{\infty} \xi_x(x)He'_m\left(\frac{\sqrt{2}(x-m)}{\sigma}\right)\frac{\sqrt[4]{2}}{\sqrt{\sigma}}e^{-\frac{(x-m)^2}{2\sigma^2}}dx,$$

Eq. 3-10

$$\xi_{n_y} = \int_{y_a}^{y_b} \xi_y(y)\tilde{L}_{n_y}(y)dy = \int_{y_a}^{y_b} \xi_y(y)L_{n_y}(y)\frac{1}{(y_b-y_a)}dy.$$

Eq. 3-11

Table 3 reports the expression of the $He_{n_x}(x)$ and $L_{n_y}(y)$ for a generalized reference system.

Table 3: Expression for the first 3 orders of Hermite polynomials.

Order	$He_{n_x}(x)$	$L_{n_y}(y)$
0	$\sqrt{2\sigma}\sqrt[4]{\pi}$	$\sqrt{(y_b-y_a)}$
1	$2\frac{\sqrt[4]{\pi}}{\sqrt{\sigma}}(x-m)$	$x\sqrt{3(y_b-y_a)}$
2	$\sqrt{2\sigma}\sqrt[4]{\pi}\left[\left(\frac{\sqrt{2}(x-m)}{\sigma}\right)^2-1\right]$	$(3x^2-1)2\sqrt{(y_b-y_a)5}$
3	$2\frac{\sqrt[4]{\pi}}{\sqrt{\sigma}}\left[\left(\frac{\sqrt{2}(x-m)}{\sigma}\right)^2-3\right](x-m)$	$(5x^3-3x)\sqrt{(y_b-y_a)7}$

3.1.2 Numerical Evaluation of the Moment Integrals

Collocation methods have the characteristic of not altering the solution scheme for $\bar{\xi}$ by introducing additional equations for the solution of its moments but rather reconstructing those moments from the knowledge of $\bar{\xi}$, with respect to predetermined values of (x, y). Essentially, collocation methods implement Gauss or Gauss-like methodologies with respect to the polynomial basis to compute the moment integrals. Here we will illustrate only the exact Gauss methodology that has been implemented into RAVEN.

Finding the Gauss point and weights is non-trivial and costly. Therefore, it is useful to use existing external libraries. RAVEN makes use of NumPy [8], which provides the points and weights for the standardized weighting and support functions. In this particular case, NumPy provides $\{\omega_i, x'_i\}$ and $\{\omega_j, y'_j\}$, which satisfy:

Legendre

$$\int_{-1}^{1} g(y')\,dy' = \sum_{i=1}^{J} \omega_j g\left(y'_j\right),$$

Hermite

$$\int_{-\infty}^{\infty} f(x')e^{\frac{x'^2}{2}}dx' = \sum_{i=1}^{I} \omega_i f(x'_i),$$

Eq. 3-12

Hermite:

The first step is to recall the coordinate transformation (Eq. 3-3) and the moment expression (Eq. 3-10):

$$x' = \frac{\sqrt{2}(x-m)}{\sigma}, \qquad or \;\; x = \frac{\sigma}{\sqrt{2}}x' + m,$$

$$\xi_{n_x} = \int_{-\infty}^{\infty} \xi_x(x) He'_m\left(\frac{\sqrt{2}(x-m)}{\sigma}\right)\frac{\sqrt[4]{2}}{\sqrt{\sigma}} e^{-\frac{(x-m)^2}{2\sigma^2}} dx.$$

Combining the two, after algebraic manipulation, it is possible to recast the integral in a form compatible with the Gauss integration formula available.

$$\begin{aligned}\xi_{n_x} &= \frac{\sqrt[4]{2}}{\sqrt{\sigma}}\frac{\sigma}{\sqrt{2}}\int_{-\infty}^{\infty} \xi_x\left(\frac{\sigma}{\sqrt{2}}x' + m\right) He'_m(x') e^{-\frac{x'^2}{4}} dx' \\ &= \frac{\sqrt{\sigma}}{\sqrt[4]{2}}\int_{-\infty}^{\infty} \xi_x\left(\frac{\sigma}{\sqrt{2}}x' + m\right) He'_m(x') e^{-\frac{x'^2}{4}} e^{\frac{x'^2}{4}} e^{-\frac{x'^2}{4}} dx' \\ &= \frac{\sqrt{\sigma}}{\sqrt[4]{2}}\int_{-\infty}^{\infty} \xi_x\left(\frac{\sigma}{\sqrt{2}}x' + m\right) He'_m(x') e^{\frac{x'^2}{4}} e^{-\frac{x'^2}{2}} dx'.\end{aligned}$$

If we assume $f(x') = \xi_x\left(\frac{\sigma}{\sqrt{2}}x' + m\right) He'_m(x') e^{\frac{x'^2}{4}}$, the quadrature formula we find is:

$$\xi_{n_x} = \frac{\sqrt{\sigma}}{\sqrt[4]{2}}\sum_{i=1}^{M_{x'}} \omega_{i,x'} \xi_x\left(\frac{\sigma}{\sqrt{2}}x_i' + m\right) He'_m(x_i') e^{\frac{x_i'^2}{4}}.$$

Eq. 3-13

In Appendix 2, an analytical test of the correctness of this derivation is reported, and the quadrature is used to integrate a few of the initial moments of the series.

Before moving forward, there is an important remark to be made on the relationship between the number of points in the quadrature and the overall accuracy of the Fourier representation of the ξ_x function. Let's replace the expansion of ξ_x in the moment integral expression:

$$\begin{aligned}\xi_{n_x} &= \int_{-\infty}^{\infty} \sum_{n'_x=0}^{N_x} \xi_{n'_x}\left(He_{n'_x}(x)\frac{1}{\sigma\sqrt{2\pi}} e^{-\frac{(x-m)^2}{2\sigma^2}}\right) He_{n_x}(x)\frac{1}{\sigma\sqrt{2\pi}} e^{-\frac{(x-m)^2}{2\sigma^2}} dx \\ &= \frac{1}{\sigma^2 2\pi}\int_{-\infty}^{\infty} \sum_{n'_x=0}^{N_x} \xi_{n'_x}\left(He_{n'_x}(x)\right) He_{n_x}(x) e^{-\frac{(x-m)^2}{\sigma^2}} \\ &= \frac{1}{\sigma^2 2\pi}\sum_{n'_x=0}^{N_x} \int_{-\infty}^{\infty} \xi_{n'_x} He_{n'_x}(x) He_{n_x}(x) e^{-\frac{(x-m)^2}{\sigma^2}} dx.\end{aligned}$$

From the last expression, we see that to compute accurately a moment of order N_x, the integrands need to be of order $2N_x$. Given the rule that relates the number of points to the order of accuracy of any Gauss rule ($2J - 1 = order$), the number of points needed are:

$$2J - 1 > 2N_x.$$

Eq. 3-14

This is a rule of general applicability for all Gauss-derived quadrature rules and thus will be not repeated for the Legendre-based rules.

Legendre:

Combining the transformation of the coordinate (Eq. 3-3) and the definition of the Gauss rule in Eq. 3-12 for the Legendre polynomials, we have:

$$\int_{-1}^{1} g(y')dy' = \sqrt{\frac{2}{(y_b - y_a)}} \int_{y_a}^{y_b} g\left(y'(y)\right) \sqrt{\frac{2}{(y_b - y_a)}} dy = \sum_{j=1}^{J} \omega_j g\left(y'(y_j)\right).$$

Posing $g\left(y'(y)\right) = \xi_{n_y}(y) L'_{n_y}\left(y'(y)\right)$:

$$\sqrt{\frac{2}{(y_b - y_a)}} \int_{y_a}^{y_b} g\left(y'(y)\right) \sqrt{\frac{2}{(y_b - y_a)}} dy = \sqrt{\frac{2}{(y_b - y_a)}} \int_{y_a}^{y_b} \xi_y(y) L'_{n_y}\left(y'(y)\right) \sqrt{\frac{2}{(y_b - y_a)}} dy$$

$$= \sqrt{\frac{2}{(y_b - y_a)}} \xi_{n_y} = \sum_{j=1}^{J} \omega_j \xi_{n_y} \left(\frac{(y_b - y_a)}{2} y'_j + \frac{(y_b + y_a)}{2} \right) L'_m(y'_j) \sqrt{\frac{2}{(y_b - y_a)}},$$

finally:

$$\xi_{n_y} = \frac{\sqrt{(y_b - y_a)}}{\sqrt{2}} \sum_{j=1}^{J} \omega_j \xi_{n_y} \left(\frac{(y_b - y_a)}{2} y'_j + \frac{(y_b + y_a)}{2} \right) L'_m(y'_j).$$

Eq. 3-15

3.1.3 Final Numerical Form

Substituting both expressions of the numerical integration of the moments (Eq. 3-13 and Eq. 3-15) into the original expansion (Eq. 3-9) yields:

$$\bar{\xi} = \xi_x \xi_y = \left[\sum_{n_x=0}^{N_x} \left(\sum_{i=0}^{M_x} \omega_i \xi_x\left(x(x'_i)\right) He_{n_x}\left(x(x'_i)\right) \right) He_{n_x}\left(x'(x)\right) e^{-\frac{(x-m)^2}{2\sigma^2}} \right]$$

$$* \left[\sum_{n_y=0}^{N_y} \left(\sum_{i=0}^{M_x} \omega_i \xi_{n_y}\left(y(y'_i)\right) L_{n_y}\left(y(y'_i)\right) \right) L_{n_y}\left(y'(y)\right) \right],$$

Eq. 3-16

or, using the polynomial expression in the reference system:

$$\bar{\xi} = \xi_x \xi_y = \left[\sum_{n_x=0}^{N_x} \left(\frac{\sqrt{\sigma}}{\sqrt[4]{2}} \sum_{i=1}^{M_{x'}} \omega_{i,x'} \xi_x \left(\frac{\sigma}{\sqrt{2}} x' + m \right) He'_m(x') e^{\frac{x'^2}{4}} \right) \left(He'_{n_x}(x') \frac{\sqrt[4]{2}}{\sqrt{\sigma}} e^{-\frac{(x-m)^2}{2\sigma^2}} \right) \right]$$
$$* \left[\sum_{n_y=0}^{N_y} \frac{\sqrt{(y_b - y_a)}}{\sqrt{2}} \sum_{j=0}^{J} \omega_{j,y} \xi_{n_y} \left(\frac{(y_b - y_a)}{2} y'_j + \frac{(y_b + y_a)}{2} \right) L'_m \left(y'_j \right) \left(L'_m(y') \sqrt{\frac{2}{(y_b - y_a)}} \right) \right].$$

Eq. 3-17

The coordinate mapping is:

$$x' = \frac{\sqrt{2}(x - m)}{\sigma}, \qquad or \;\; x = \frac{\sigma}{\sqrt{2}} x' + m,$$
$$y' = \frac{2y - (y_b + y_a)}{(y_b - y_a)}, or \;\; y = \frac{(y_b - y_a)}{2} y' + \frac{(y_b + y_a)}{2}.$$

Eq. 3-18

3.1.4 Mean Values

Starting with the definition of mean value and the definition of the orthonormal polynomials, we can verify the relationship of the zeroth order moment and the mean value of the system response, as computed in Eq. 2-10.

Hermite:

$$\widetilde{He}_0(x) = \frac{\sqrt{\sigma 2\pi \sqrt{2}}}{\sqrt[4]{2\pi}} \frac{1}{\sigma\sqrt{2\pi}} e^{-\frac{(x-m)^2}{2\sigma^2}}, \qquad pdf(x) = \frac{1}{\sigma\sqrt{2\pi}} e^{-\frac{(x-m)^2}{2\sigma^2}}$$
$$E[\xi_x] = \int_{-\infty}^{\infty} \xi_x pdf(x) dx = \int_{-\infty}^{\infty} \xi_x \frac{1}{\sigma\sqrt{2\pi}} e^{-\frac{(x-m)^2}{2\sigma^2}} dx = \int_{-\infty}^{\infty} \xi_x \widetilde{He}_0(x) \frac{\sqrt[4]{2\pi}}{\sqrt{\sigma 2\pi\sqrt{2}}} dx$$
$$= \frac{\sqrt[4]{2\pi}}{\sqrt{\sigma 2\pi\sqrt{2}}} \int_{-\infty}^{\infty} \sum_{n_x=0}^{N_x} \xi_{n_x} \widetilde{He}_n(x) \widetilde{He}_0(x) dx = \frac{\xi_{0_x}}{\sqrt{\sigma 2\sqrt{\pi}}} = \xi_{0_x} \sqrt{S_x}.$$

Eq. 3-19

Legendre:

$$E[\xi_y] = \int_{y_a}^{y_b} \xi_y pdf(y)dy = \int_{y_a}^{y_b} \xi_y \frac{1}{(y_b - y_a)} dy = \frac{1}{\sqrt{(y_b - y_a)}} \int_{y_a}^{y_b} \xi_y \frac{1}{\sqrt{(y_b - y_a)}} dy$$
$$= \frac{1}{\sqrt{(y_b - y_a)}} \int_{y_a}^{y_b} \xi_y \widetilde{L_0}(y)dy = \frac{1}{\sqrt{(y_b - y_a)}} \xi_{y,0} = \xi_{y,0} \sqrt{S_y}.$$

Eq. 3-20

4. Application

Given the final goal of the RAVEN project, stochastic polynomials are tested with respect to their capability to properly forecast the mean value and system response in low probability regions. The accuracy of the polynomial representation of the system response is tested for a large range of values of the input space (large variation of the input parameters $\bar{\xi}$). In particular, its capability to predict the location of an iso-surface is analyzed, where the system response is constant and equal to an imposed value for any variation of the input parameters within such surface ($U(\bar{\xi}) = constant$). When it divides the input space in two regions—one leading to an output space that implies failure of the system, one leading to safer outcomes (i.e. limit surface)—this iso-surface has a special meaning and relevance to the RAVEN project. The specific physical problem is described in the following paragraphs along with the modeling choices and discussion of the results. In this case, the response of the system will be represented by the maximum clad temperature achieved ($U(\bar{\xi}) = T_{\underset{Clad}{Max}}$), and the limit surface will be the region of the space where this value is equal to the clad failure temperature ($T_{\underset{Clad}{Max}} = T_{\underset{Clad}{Failure}}$).

4.1 Case Description

In order to test the capabilities introduced with the new Stochastic Polynomial approach, a simplified PWR probabilistic risk analysis (PRA) scenario is considered. Figure 1 shows the scheme of the PWR model.

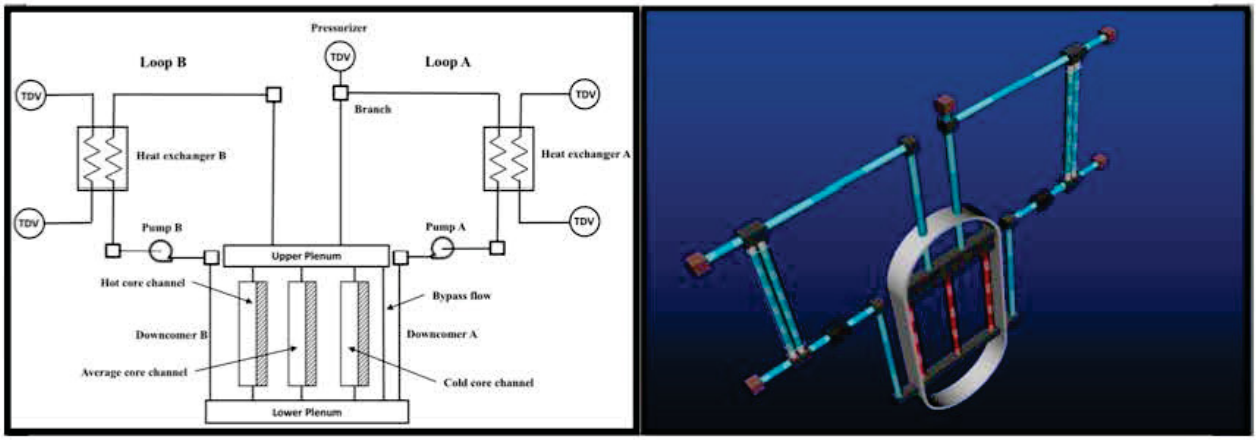

Figure 1: PWR model scheme.

The reactor vessel model consists of the down-comers, the lower plenum, the reactor core model, and the upper plenum. Core channels (flow channels with heat structure attached to each of them) are used to describe the reactor core. The core model consists of three parallel core channels and one bypass flow channel. There are two primary loops (i.e., loop A and loop B). Each loop consists of the hot leg, a heat exchanger and its secondary side pipes, the cold leg, and a primary pump. A pressurizer is attached to the loop A piping system to control the system pressure. A time dependent volume (pressure boundary conditions) component is used to represent the pressurizer. Since the RELAP-7 code two-phase flow capability is not being used for this test, single-phase, counter-current heat exchanger models are implemented to mimic the function of steam generators in order to transfer heat from the primary to the secondary loop.

4.2 Station Blackout (SBO) Scenario

The simulation of an SBO initiating event required the introduction, in the control logic, of several

components (see Figure 2), including:

- Set of three diesel generators (DGs) and associated emergency buses
- Primary power grid line 138 KV (connected to the Normal Station Supply Transformer switchyard)
- Auxiliary power grid line 69 KV (connected to the Reserve Station Service Transformer [RSST] switchyard)
- Electrical buses: 4160 V (step down voltage from the power grid and voltage of the electric converter connected to the DGs) and 480 V for actual reactor components (e.g., reactor cooling system).

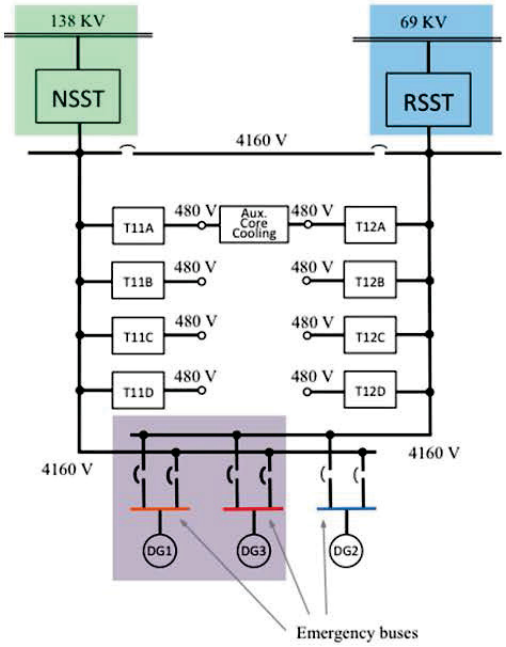

Figure 2: Scheme of the electrical system of the PWR model.

The scenario is the following:

- An external event causes a loss of off-site power due to damage of the 138 kV line and RSST switchyard. The reactor successfully scrams, and thus, power generated in the core follows the characteristic exponential decay curve.
- The set of DGs fails to start, and hence, conditions of SBO are reached (4160 V and 480 V buses are not energized). All cooling systems are subsequently off-line.
- Without the ability to cool the reactor core, its temperature starts to rise.
- In order to recover alternating current electric power on the 4160 V and 480 V buses, two recovery teams are assembled with the following strategy:
  - Recovery Team 1 focuses on the recovery of the DGs. Due to internal damage at the DG building, two DGs (i.e., DG1 and DG3) need to be repaired (see Figure 3[a]).
  - Recovery Team 2 focuses on the recovery of the RSST switchyard. 69kV line is energized, but the RSST switchyard needs to be recovered (see Figure 3[b]).
  - Meanwhile, the owning company is working on the restoration of the primary 138 kV line (see Figure 3[c]).
  - When the 4160 V buses are energized (through the recovery of the DGs, RSST, or 138kV line), the auxiliary cooling system is able to cool the reactor core down, and thus, core temperature decreases.

Because of the uncertainties associated with the recovery of both of the DGs, the RSST, and the 138KV line, a stochastic model should be used to represent these events. Given the time scale associated with the dynamics of the RELAP-7 PWR model, the corresponding probability distribution functions are as follows:

- DGs: Team 1 is required to gather a dead time of 100s at the DGs building, and DG1 repair time (T_{DG1}) has a normal distribution, having mu = 800 and sigma = 200. This distribution is also truncated such that $0 < T_{DG1} < 2500$. The recovery time of DG3, T_{DG3}, is proportional to T_{DG1}. Such relation has been modeled using multiplication factor T_{12} (i.e., $T_{DG3} = T_{DG1} \times T_{12}$). T_{12} is uniformly distributed between [0.5 1].
- RSST: a dead time of 400s is needed to assess the damage at the RSST switchyard and to plan its recovery. Recovery time for RSST, T_{RSST}, is normally distributed with mu = 1400 and sigma = 400.
- 138KV line: the recovery of the main alternating current line, T_{138}, is normally distributed with mu = 2000 and sigma = 500.

In addition, the clad failure temperature is not fixed, but it is probabilistically distributed with a triangular distribution characterized by the following parameters:

- mode: xPeak = 2200 F(1477.59 K), 10 Code of Federal Regulations regulatory limit
- lower bound: xMin = 1800 F (1255.37 K), PRA success criterion
- upper bound: xMax = 2600(1699.82 K), Urbanic-Heidrick transition temperature.

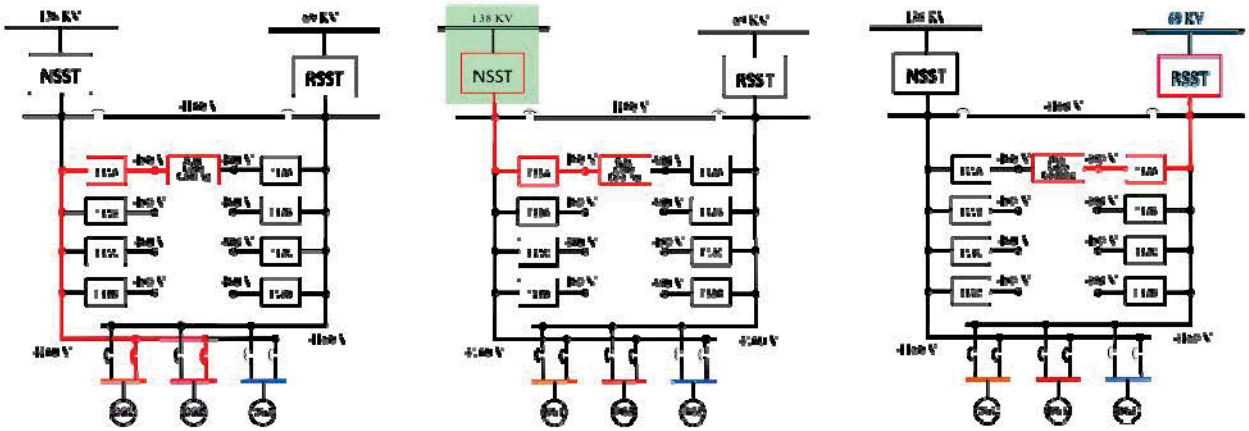

Figure 3: Alternating current power recovery paths through: DGs (a), RSST (b) and 138 kV line (c). Red lines indicate electrical path to power Aux cooling system.

4.3 Analysis of Stochastic Polynomial Performance

Classically stochastic polynomials are used to compute mean and higher order statistical moments of the response (in our case the T_{Clad}^{Max}). While this is the information usually necessary and sufficient to perform system optimization and data assimilation, it does not cover every need in the case of safety related analysis. In fact, high-risk situations are usually present far away from the mean value of the system response. For these types of analyses, it is important to evaluate the fidelity of the polynomial representation far away from the region of the response mean.

After performing a few analytical tests, it was immediately made clear that the convergence in the dμ measure was incapable of effectively controlling the error over the estimation of the system response when not weighted by the probability. This could also be inferred from the fact that in the Hermite-based interpolation, the overall weight of the error decays exponentially while moving away from the region of the mean value of the response.

For this reason, usage of fast decaying weighting functions currently seems inappropriate in PRA. Legendre-based interpolation does not have this disadvantage, given the fact that it uses the standard norm. Unfortunately, for the moment, RAVEN implements the standard stochastic polynomial approach where the polynomial interpolating functions are the ones that are orthonormal, with respect to the square of the probability distribution function (like Hermite for normal distribution). So, it is not currently possible to use Legendre-based approximation while having the input parameter values normally distributed.

For this reason, aware of the poor results that would be obtained in evaluating the limit surface using Hermite-based polynomials, all the input parameter distributions have been switched to uniform distributions (characterized by the same mean of the corresponding normal distribution) to use Legendre-based interpolation.

Moreover, two different mathematical representations of the original physical problem were analyzed. This is due to some difficulties, which were highlighted during the analysis of the results, in the representation of discontinuous system by the stochastic polynomials. This issue will be discussed more in detail in the following paragraphs.

4.4 First Set of Tests

The initial test was performed using third order Legendre interpolating polynomials that, in accord with Eq. 2.35, requires $4^4 = 256$ system evaluations to complete the quadrature formula.
The mean value of the polynomial approximation of system response is then compared with the mean obtained from 400 Monte Carlo sampling of original system.
More details:

- Input parameters sampled:
  - t_{DG1}: recovery time of the first DG auxiliary system
  - t_{DG3}: recovery time of the third DG auxiliary system
  - t_{RSST}: recovery time of the auxiliary power line
  - t_{T138}: recovery time of the main power line
  - $T_{\substack{Failure \\ Clad}}$: failure temperature of the clad. This parameter is sampled posterior, and therefore excluded from the dimension of the input space.
- 400 different RELAP-7 inputs have been generated by Monte Carlo sampling of the input space. The outcomes are used to forecast the mean of $T_{\substack{Max \\ Clad}}$, the location of the limit surface ($T_{\substack{Max \\ Clad}} = T_{\substack{Failure \\ Clad}}$), and an overall characterization of the system response.
- The moments needed for a third order complete representation of the system response, with respect to a Legendre polynomial base, are computed by a quadrature rule coming from a full tensor product of 4 mono-dimensional quadratures with respect to the variables t_{DG1}, t_{DG3}, t_{RSST}, and t_{T138}.
- The same 400 inputs, generated by the Monte Carlo, are then used to sample the response of the system approximated by its polynomial representation. The outcome is then used to perform a one to one comparison with the results from the initial Monte Carlo on the real system. The mean value is computed directly using Eq. 3-20.

The mean value of the maximum clad temperature computed by the stochastic polynomials is 1006.5 K

versus 1071.6 K computed by the Monte Carlo. Using the central limit theorem, the probability that the mean value computed by the Monte Carlo is the exact one given by a normal distribution with $\sigma = \frac{1}{\sqrt{N}} = \frac{1}{\sqrt{400}} = 5\%$. As a consequence, the probability of being the exact mean value, the one coming from the polynomial approximation, is compatible with a 20 % probability.

In the scenario accident considered, the time evolution of the maximum clad temperature is independent from the system recovery sequence and is uniquely determined by the moment the first recovered system gets back online. As a consequence, the mapping from the recovery times (any of the ones considered) to the maximum clad temperature could be represented by a mapping between the minimum of the recovery times and the maximum clad temperature:

$$T_{\underset{Clad}{Max}} = T_{\underset{Clad}{Max}}(t_{DG1}, t_{DG3}, t_{RSST}, t_{T138})$$

$$T_{\underset{Clad}{Max}} = T_{\underset{Clad}{Max}}\left(t_{min} = min(t_{DG1}, t_{DG3}, t_{RSST}, t_{T138})\right)$$

From the last equation, it is clear that the representation of $T_{\underset{Clad}{Max}}$ as a function of $(t_{DG1}, t_{DG3}, t_{RSST}, t_{T138})$ is at most of class C_0, since the change of coordinate $t_{min} = min(t_{DG1}, t_{DG3}, t_{RSST}, t_{T138})$ is of class C_0. This is a strong indication that a continuous polynomial representation of the system response is going to be difficult. In fact, this is evident when comparing Figure 3 versus Figure 4. In those figures, for the Monte Carlo sampling of the stochastic polynomial representation and of the real system, the max clad temperature is represented as a function of t_{min}. It is clear that the polynomial representation has failed to match the system response. No further analysis has been performed given the low quality of the results.

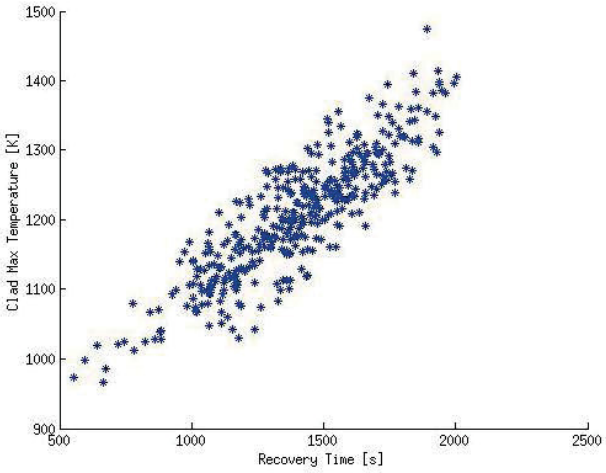

Figure 3: Max clad temperature as a function of t_{min} obtained while sampling the system polynomial representation.

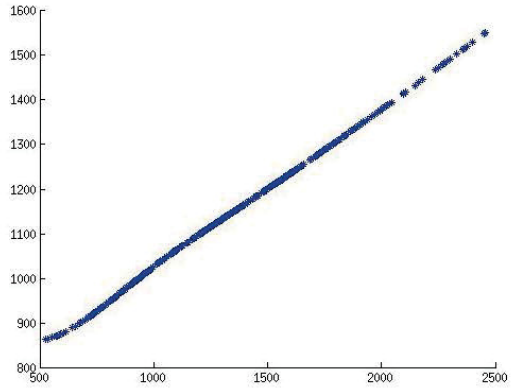

Figure 4: Max clad temperature as a function of t_{min} for the original system.

4.5 Revisited Test Strategy

As already pointed out, the maximum clad temperature is a function of the instant at which the first recovered system gets back online. Consequently, it would make sense to consider only this variable when seeking to approximate the system response.
For this case the two uncertain parameters are:

- t_{min}: minimal time of recovery of any of the auxiliary system
- $T_{\substack{Failure \\ Clad}}$: failure temperature of the clad. This parameter is sampled posterior, and therefore excluded from the dimension of the input space

For the arguments previously mentioned, the system characterization (maximum clad temperature as a function of the minimum of the recovery times) of the Monte Carlo would be unaltered, just its sampling density would change. As a consequence, the profile illustrated in Figure 4 will remain valid. The new profile obtained by the sampling of the polynomial approximation of the system (mono-dimensional quadrature with four Gauss-Legendre points) is reported in Figure 5. Clearly, the improvement is noticeable. This is also confirmed by Table 4, where the mean value comparison is reported. Figures 6 and 7 show the limit surface in the two-dimensional space of the maximum clad temperature and clad failure temperature, respectively, obtained by a Monte Carlo sampling of the real system (RELAP-7) and of its polynomial approximation. While numerical differences are still noticeable, the polynomial approximation is, at least qualitatively, capable to represent the system response.

Table 4: Maximum Clad Temperature Mean value.

$mean_{MonteCarlo}$	$mean_{StochasticPolynomials}$	$sigma_{mean\text{-}MonteCarlo}$	r.e.
1143.91 K	1185.65 K	5.0 %	3.65%

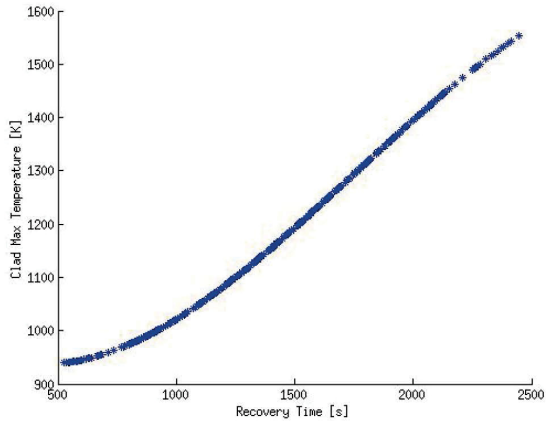

Figure 5: Stochastic Polynomials max clad temperature (2 uncertain parameters).

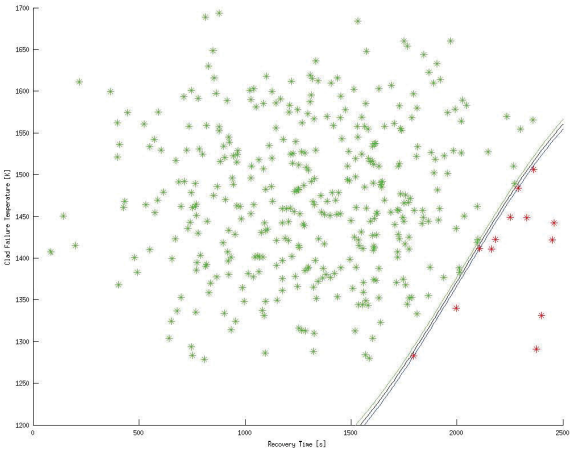

Figure 6: Limit surface from the Monte Carlo sampling of the original system.

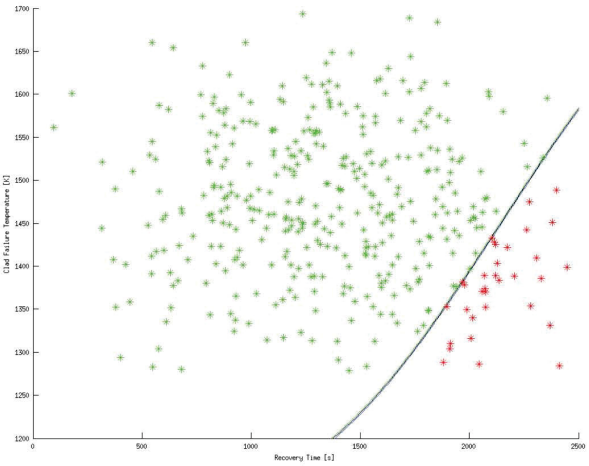

Figure 7: Limit surface from the Monte Carlo sampling of polynomial approximation.

5. Conclusions

The milestone of performing a PRA demo using the Stochastic Polynomial Approach has been fully achieved. The two sets of calculations performed contributed to the testimony of the good implementation of the methodology and its intrinsic limitations. Further research is needed to address the main deficiency highlighted during this initial research stage. First, Legendre interpolation of the system response should be made available for all types of distribution. Second, a discontinuous decomposition of the input space should be performed to address the challenge represented by discontinuous mappings. Third, an approach to eliminate inactive regions of the input space should be considered.

6. References

1. R. W. Youngblood, V. A. Mousseau, D. L. Kelly, and T. N. Dinh, "Risk-Informed Safety Margin Characterization (RISMC): Integrated Treatment of Aleatory and Epistemic Uncertainty in Safety Analysis," *The 8th International Topical Meeting on Nuclear Thermal-Hydraulics, Operation and Safety (NUTHOS-8)* Shanghai, China, October 10–14, 2010
2. "Light Water Reactor Sustainability Program Integrated Program Plan, Revision 1," INL/EXT-11-23452, April 2013
3. D. Anders, R. Berry, D. Gaston, R. Martineau, J. Peterson, H. Zhang, H. Zhao, and L. Zou, "RELAP-7 Level 2 Milestone Report: Demonstration of a Steady State Single Phase PWR Simulation with RELAP-7," INL/EXT-12-25924, May 2012
4. C. Rabiti, A. Alfonsi, D. Mandelli, J. Cogliati, R. Martineau, C. Smith, "Deployment and Overview of RAVEN Capabilities for a Probabilistic Risk Assessment Demo for a PWR Station Blackout," INL/EXT-13-29510, June 2013
5. A. Alfonsi, C. Rabiti, D. Mandelli, J. Cogliati, R. Kinoshita, "Dynamic Event Tree Approach Level III Milestone," INL/EXT-13-30332, October 2013
6. D. Xiu, G. Karniadakis, "The Wiener-Askey Polynomial Chaos for Stochastic Differential Equations," *SIAM Journal on Scientific Computing*, **24**, 2, pp. 619–644 (2002)
7. M. S. Eldred, "Recent Advances in Non-Intrusive Polynomial Chaos and Stochastic Collocation Methods for Uncertainty Analysis and Design," *50th Structures, Structural Dynamics, and Materials Conference* Palm Springs, California, May 4–7, 2009, Palm Springs, California
8. T. E. Oliphant, "Python for Scientific Computing," *Computing in Science & Engineering* **9**, 3, pp. 10–20 (2007)

7. Appendixes

7.1 Appendix 1: Orthonormal Test of the Hermite Polynomial in the Actual System

From the expression of the Hermite polynomials in the actual system, given (Eq. 3-5) as a function of the Hermite polynomials in the standard system reported in Table 2, it is possible to write:

$$He_0(x) = \frac{\sqrt{\sigma 2\pi\sqrt{2}}}{\sqrt[4]{2\pi}}$$

$$He_1(x) = \frac{\sqrt{2}(x-m)}{\sigma}\frac{\sqrt{\sigma 2\pi\sqrt{2}}}{\sqrt[4]{2\pi}}$$

Now the following tests will be performed:

1. $\int_{-\infty}^{\infty} He_0(x)He_0(x)\frac{1}{\sigma^2 2\pi}e^{-\frac{(x-m)^2}{\sigma^2}}dx = 1$
2. $\int_{-\infty}^{\infty} He_0(x)He_1(x)\frac{1}{\sigma^2 2\pi}e^{-\frac{(x-m)^2}{\sigma^2}}dx = 0$
3. $\int_{-\infty}^{\infty} He_1(x)He_1(x)\frac{1}{\sigma^2 2\pi}e^{-\frac{(x-m)^2}{\sigma^2}}dx$

Test 1

$$\int_{-\infty}^{\infty} He_0(x)He_0(x)\frac{1}{\sigma^2 2\pi}e^{-\frac{(x-m)^2}{\sigma^2}}dx = \int_{-\infty}^{\infty}\frac{\sqrt{\sigma 2\pi\sqrt{2}}}{\sqrt[4]{2\pi}}\frac{\sqrt{\sigma 2\pi\sqrt{2}}}{\sqrt[4]{2\pi}}\frac{1}{\sigma^2 2\pi}e^{-\frac{(x-m)^2}{\sigma^2}}dx$$
$$= \int_{-\infty}^{\infty}\frac{\sigma 2\pi\sqrt{2}}{\sqrt{2\pi}}\frac{1}{\sigma^2 2\pi}e^{-\frac{(x-m)^2}{\sigma^2}}dx = \int_{-\infty}^{\infty}\frac{1}{\sigma\sqrt{\pi}}e^{-\frac{(x-m)^2}{\sigma^2}}dx = 1$$

Test 2

$$\int_{-\infty}^{\infty} He_0(x)He_1(x)\frac{1}{\sigma^2 2\pi}e^{-\frac{(x-m)^2}{\sigma^2}}dx = \int_{-\infty}^{\infty}\frac{\sqrt{\sigma 2\pi\sqrt{2}}}{\sqrt[4]{2\pi}}\frac{\sqrt{2}(x-m)}{\sigma}\frac{\sqrt{\sigma 2\pi\sqrt{2}}}{\sqrt[4]{2\pi}}\frac{1}{\sigma^2 2\pi}e^{-\frac{(x-m)^2}{\sigma^2}}dx$$
$$= \int_{-\infty}^{\infty}\frac{\sqrt{2}}{\sqrt{2\pi}}\frac{\sqrt{2}(x-m)}{1}\frac{1}{\sigma^2}e^{-\frac{(x-m)^2}{\sigma^2}}dx = \frac{\sqrt{2}}{\sigma^2\sqrt{\pi}}\int_{-\infty}^{\infty}(x-m)e^{-\frac{(x-m)^2}{\sigma^2}}dx$$
$$= \frac{\sqrt{2}}{\sigma^2\sqrt{\pi}}\left(\int_{-\infty}^{\infty}xe^{-\frac{(x-m)^2}{\sigma^2}}dx - m\int_{-\infty}^{\infty}e^{-\frac{(x-m)^2}{\sigma^2}}dx\right)$$
$$= \frac{\sqrt{2}}{\sigma^2\sqrt{\pi}}\left(\int_{-\infty}^{\infty}(y+m)e^{-\frac{y^2}{\sigma^2}}dy - m\sqrt{\pi}\sigma\right) = \frac{\sqrt{2}}{\sigma^2\sqrt{\pi}}\left(\int_{-\infty}^{\infty}ye^{-\frac{y^2}{\sigma^2}}dy + m\sqrt{\pi}\sigma - m\sqrt{\pi}\sigma\right)$$
$$= \frac{\sqrt{2}}{\sigma^2\sqrt{\pi}}\left(\int_{0}^{\infty}ye^{-\frac{y^2}{\sigma^2}}dy + \int_{-\infty}^{0}ye^{-\frac{y^2}{\sigma^2}}dy\right) = \frac{\sqrt{2}}{\sigma^2\sqrt{\pi}}\left(\int_{0}^{\infty}ye^{-\frac{y^2}{\sigma^2}}dy + \int_{\infty}^{0}y'e^{-\frac{y'^2}{\sigma^2}}dy'\right)$$
$$= 0$$

Test 3

$$\int_{-\infty}^{\infty} He_1(x)He_1(x)\frac{1}{\sigma^2 2\pi}e^{-\frac{(x-m)^2}{\sigma^2}}dx$$

$$= \int_{-\infty}^{\infty} \frac{\sqrt{2}(x-m)}{\sigma}\frac{\sqrt{\sigma 2\pi\sqrt{2}}}{\sqrt[4]{2\pi}}\frac{\sqrt{2}(x-m)}{\sigma}\frac{\sqrt{\sigma 2\pi\sqrt{2}}}{\sqrt[4]{2\pi}}\frac{1}{\sigma^2 2\pi}e^{-\frac{(x-m)^2}{\sigma^2}}dx$$

$$= \frac{2}{\sqrt{\pi}\sigma^3}\int_{-\infty}^{\infty}(x-m)^2 e^{-\frac{(x-m)^2}{\sigma^2}}dx = \frac{2}{\sqrt{\pi}\sigma^3}\int_{-\infty}^{\infty} y^2 e^{-\frac{y^2}{\sigma^2}}dx = \frac{2}{\sqrt{\pi}\sigma^3}2\sqrt{\pi}2\frac{\sigma^3}{2^3} = 1$$

7.2 Appendix 2: Test of the Translation Rule for the Gauss-Hermite Quadrature

The purpose of this test is to verify that if $\xi_x(x) = \widetilde{He}_1(x)$, then its projection properly leads to $\xi_{0_x} = 0$ and $\xi_{1_x} = 1$. For doing so, we are going to use the Gauss-Hermite quadrature for which points and weight are given in Table 55.

Table 5: Points and Weights for the Gauss-Hermite quadrature formula

Points	Coordinate	Weight
2	± 1	$\frac{\sqrt{\pi}}{\sqrt{2}}$
3	0	$\frac{2\sqrt{\pi}}{3}\sqrt{2}$
	$\pm\sqrt{3}$	$\frac{\sqrt{\pi}}{3\sqrt{2}}$

The problem could be formulated as follows:

Given: $\xi_x = \xi_{1_x}\left(He_1'\left(\frac{\sqrt{2}(x-m)}{\sigma}\right)\frac{\sqrt[4]{2}}{\sqrt{\sigma}}e^{-\frac{(x-m)^2}{2\sigma^2}}\right)$ verify

1. $\xi_0 = \frac{\sqrt{\sigma}}{\sqrt[4]{2}}\sum_{i=1}^{3}\omega_{i,x'}\xi_x\left(\frac{\sigma}{\sqrt{2}}x' + m\right)He_0'(x')e^{\frac{x'^2}{4}} = 0$
2. $\xi_1 = \frac{\sqrt{\sigma}}{\sqrt[4]{2}}\sum_{i=1}^{3}\omega_{i,x'}\xi_x\left(\frac{\sigma}{\sqrt{2}}x' + m\right)He_1'(x')e^{\frac{x'^2}{4}} = 1$

It is convenient first to reformulate the Gaussian quadrature as follows:

$$\xi_{n_x} = \frac{\sqrt{\sigma}}{\sqrt[4]{2}} \sum_{i=1}^{3} \omega_{i,x\prime} \xi_x \left(\frac{\sigma}{\sqrt{2}} x_i{}' + m \right) He'_n(x_i{}') e^{\frac{x_i{}'^2}{4}}$$

$$= \frac{\sqrt{\sigma}}{\sqrt[4]{2}} \sum_{i=1}^{3} \omega_{i,x\prime} \left[\sum_{n\prime_x=0}^{N_x} \xi_{n\prime_x} \left(He'_n(x_i{}') \frac{\sqrt[4]{2}}{\sqrt{\sigma}} e^{-\frac{x_i{}'^2}{4}} \right) \right] He'_m(x_i{}') e^{\frac{x\prime^2}{4}}$$

$$= \sum_{i=1}^{3} \omega_{i,x\prime} \left[\sum_{n\prime_x=0}^{N_x} \xi_{n\prime_x} \left(He'_n(x_i{}') \right) \right] He'_m(x_i{}') = \sum_{i=1}^{3} \omega_{i,x\prime} \left[\xi_{1_x} \left(He'_1(x_i{}') \right) \right] He'_m(x_i{}') \, \xi_{m_x}$$

$$= \frac{1}{\sqrt[4]{2\pi}} \sum_{i=1}^{3} \omega_{i,x\prime} x'_i He_{m_x}(x'_i)$$

The desired results follow immediately:

$$\xi_{0_x} = \frac{1}{\sqrt[2]{2\pi}} \left(\sqrt{3} - \sqrt{3} \right) \frac{\sqrt{\pi}}{3\sqrt{2}}$$

$$\xi_{1_x} = \frac{1}{\sqrt[2]{2\pi}} \sum_{i=1}^{3} \omega_{i,x\prime} x'_i x'_i = \frac{1}{\sqrt[2]{2\pi}} 3 \frac{\sqrt{\pi}}{3\sqrt{2}} 2 = 1$$